

Coarse-to-Fine Video Denoising with Dual-Stage Spatial-Channel Transformer

Wulian Yun, Mengshi Qi, Chuanming Wang, Huiyuan Fu, Huadong Ma
Beijing University of Posts and Telecommunications
Beijing, China

ABSTRACT

Video denoising aims to recover high-quality frames from the noisy video. While most existing approaches adopt convolutional neural networks (CNNs) to separate the noise from the original visual content, however, CNNs focus on local information and ignore the interactions between long-range regions. Furthermore, most related works directly take the output after spatio-temporal denoising as the final result, neglecting the fine-grained denoising process. In this paper, we propose a Dual-stage Spatial-Channel Transformer (DSCT) for coarse-to-fine video denoising, which inherits the advantages of both Transformer and CNNs. Specifically, DSCT is proposed based on a progressive dual-stage architecture, namely a coarse-level and a fine-level to extract dynamic feature and static feature, respectively. At both stages, a Spatial-Channel Encoding Module (SCEM) is designed to model the long-range contextual dependencies at spatial and channel levels. Meanwhile, we design a Multi-scale Residual Structure to preserve multiple aspects of information at different stages, which contains a Temporal Features Aggregation Module (TFAM) to summarize the dynamic representation. Extensive experiments on four publicly available datasets demonstrate our proposed DSCT achieves significant improvements compared to the state-of-the-art methods.

1 INTRODUCTION

Video denoising is a fundamental task in computer vision, which aims to reconstruct clean frames from the noisy video, as shown in Figure 1. It has attracted considerable research interests because the video denoising can greatly influence the recognition and understanding of video data by subsequent down-stream tasks, such as vintage film remastering, video surveillance, *et al.*

Different from the image denoising [9, 18, 26] tasks that focus on the extracting spatial information in the image, the video denoising pays more attention to the spatial information as well as the temporal representation from the video sequence. Therefore, existing methods began to utilize the spatio-temporal information for video denoising. For example, V-BM4D [3] searched similar patches in both the spatial and temporal dimensions, while FastDVDnet [2] utilized the U-Net architecture [19] to process information at both the spatial and temporal level. However, these methods process the spatio-temporal information in a hybrid manner, and ignore the spatial noise distribution and temporal deformation. Moreover, these methods only implement the coarse-grained level denoising, but not perform the fine-grained job.

Nowadays, the CNN-based methods [2, 21, 23, 25, 33, 34] become the mainstream method for video denoising. However, these CNN-based methods have limitations for capturing long-range relations, because of the intrinsic locality of the convolutional kernel. Alternatively, transformer adopts the self-attention mechanism to capture

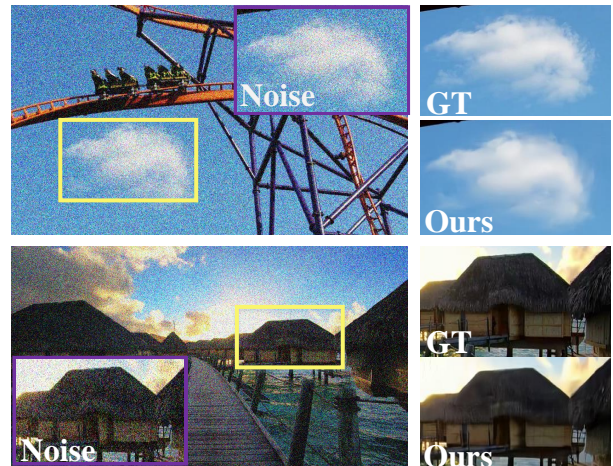


Figure 1: Illustration of the video denoising task. From left to right, we show the noisy frames in videos, ground truth clean frames and the predicted results of our proposed method.

global contextual relationships and have been shown good performance in nature language processing and computer vision field. Therefore, it is worthy to exploring how to inherit the advantages of CNN and transformer for video denoising.

In this study, we propose an end-to-end Dual-stage Spatial-channel Transformer (DSCT) for coarse-to-fine video denoising. Specifically, DSCT contains a *coarse-level stage* and a *fine-level stage*: the *coarse-level stage* aims to extract the dynamic feature from neighbor frames to obtain the coarse-grained denoising result, while the *fine-level stage* transfers the coarse-grained result into the fine-grained clean one by exploiting the static feature. During the both stages, the Spatial-Channel Encoding Module (SCEM) is introduced to capture the global contextual information from both spatial position and channels. Moreover, a *Multi-Scale Residual Structure* is designed to preserve the multi-scale information during both stages, including the temporal information at the *coarse-level stage*, the low-level spatial features and high-level semantic representation at the *fine-level stage*, and intermediate-level context information between the *coarse-level stage* and *fine-level stage*. Additionally, we design a Temporal Features Aggregation Module (TFAM) to summarize the dynamic representation from video sequence, and a Spatial-Channel Encoding Module to achieve other scales information.

The contributions of this paper can be summarized as follows:

- We propose a novel dual-stage framework for video denoising that gradually obtains the high-quality clean video frames in a coarse-to-fine manner.
- We design a Spatial-Channel Transformer to simultaneously capture both the local information and global contextual dependencies between neighbour frames, which contains a Spatial-Channel Encoding Module to extract long-range spatial-channel information.
- We introduce a Multi-Scale Residual Structure to maintain the multiple aspects of information in different stages, and further enhance the representation in each level by adopting skipping residual connections.

To verify the effectiveness and superiority of the proposed DSCT, we conduct extensive experiments on four widely-adopted public available datasets, *i.e.*, Davis, Set8, Vimeo90k, Raw Videos. The experimental results demonstrate that our model achieves state-of-the-art performance.

2 RELATED WORK

2.1 Video Denoising

Existing video denoising methods can be mainly divided into three categories, including patch-based traditional methods [3, 24], explicit motion compensation methods [21, 22] and non-explicit motion compensation methods [2, 25, 33]. As an example, V-BM4D [3] was a representative of the patch-based method, which extended the image denoising method BM3D [18] to video level. VNLB [24] was similar to V-BM4D, but its computation time is too longer to be applied in practice.

With the development of neural networks, deep learning based video denoising methods are proposed in recent years. The first neural network-based method [23] used Recurrent Neural Networks (RNNs) for gray-scale image denoising. Xue et al.[22] proposed TOFlow to extract a purpose-built flow representation through aligning frames via CNN. VNLnet [25] applied CNN to video denoising and used the similarity search strategy for non-local patches processing. Claus et al. [33] proposed ViDeNN, which performs blind noise processing in both the spatial and temporal level. DVDnet [21] followed independent spatial and temporal steps to model the motion relationship between adjacent frames. Subsequently, FastDVDnet [2] extended DVDnet through adding optical flow prediction based on the U-Net [19]framework. Vaksmanet et al. [11] proposed PaCNet, which introduced patch-craft frames and self-similarity to denoise the video. Yue et al. [28]proposed RViDeNet to remove real noise using spatial, channels and temporal correlations. UDVD [27] combines U-Net [19] and blind-spot [12] network without any explicit motion compensation.

Existing methods mainly use CNNs to extract features, neglecting the long-range context dependencies in video frames. Therefore, we propose a new method to inherit the advantages of both Transformer and CNNs to capture both global and local information. In addition, we formulate the video denoising task as coarse-to-fine denoising problem to fully exploit the spatial-temporal information between video frames and further refine the the coarse denoising results to fine-grained ones.

2.2 Vision Transformer

Transformer[31] was first proposed to solve the machine translation problem in natural language processing (NLP). Since the transformer can capture long-range dependencies in data with self-attention mechanism, it can obtain more global information. Therefore, significant efforts have been made to introduce Transformer to computer vision field [6, 7, 13, 14, 20, 29, 32, 35, 37]. For example, Kolesnikov et al. [32] utilized transformer for image recognition on the ImageNet dataset. Liu et al. [37] proposed swin transformer to construct hierarchical structure using sliding window operation. Chen et al. [30] proposed IPT for various restoration down-stream tasks by jointly training Standard Transformer blocks with multiple tails and heads. Wang et al. [17] proposed a U-Net based architecture with LeWin Transformer block for image restoration tasks such as denoising and deblurring. Transformer [7, 17, 30] has been designed for image denoising tasks, but very few is designed for video denoising. In this paper, we propose a Spatial-Channel Transformer, which takes full advantages of the transformer to capture global features in both spatial and temporal dimensions.

3 METHODOLOGY

In this work, we propose a Dual-stage Spatial-Channel Transformer (DSCT) for video denoising, as shown in Figure 2. DSCT mainly consists of two stages: *coarse-level* stage and *fine-level* stage. The *coarse-level stage* aims at extracting dynamic features from spatio-temporal dimensions of neighbor frames, and then produce the coarse-grained denoising results. While the *fine-level stage* focuses on static feature extraction from the coarse-grained denoising results, and generate the boosted fine-grained denoising outputs. In addition, we design a *multi-scale residual structure* to maintain the multi aspects of information in different stages. Note that both stages can be jointly optimized in an end-to-end training architecture.

Problem Definition: Given a training set $\mathcal{I} = \{\tilde{\mathbf{I}}_i, \mathbf{I}_i\}_{i=1}^N$, where $\tilde{\mathbf{I}}_i$ denotes the i -th noise video frame in \mathcal{I} , \mathbf{I}_i is clean frames, and N is the number of \mathcal{I} . Our goal is to train a video denoising model based on \mathcal{I} , which can transfer each noise frame $\tilde{\mathbf{I}}$ into the clean one \mathbf{I} .

3.1 Coarse-Level Stage

We firstly adopt an encoder-decoder architecture during the *coarse-level stage* to extract the dynamic features from multiple video frames. The *coarse-level stage* is comprised of Multi-frame Encoder Module and Decoder Module, in which the encoder is used to extract the global and local features of each noisy frame by the Spatial-Channel Encoding module and the CNN. While the Decoder Module is adopted to aggregate the encoded multi-scale features, and transfer them into the coarse-grained denoised results via the CNN and upsample operation.

During this stage, we take the noisy frames set $\{\tilde{\mathbf{I}}_{i-1}, \tilde{\mathbf{I}}_i, \tilde{\mathbf{I}}_{i+1}\}$ as the input, where $\tilde{\mathbf{I}} \in \mathbb{R}^{H \times W \times C}$ (H , W and C indicate the height, width and input channel number of the frames, respectively). For simplicity, we denote $\tilde{\mathbf{I}}_i$ as the frame that needs to be denoised, while the others $\tilde{\mathbf{I}}_{i-1}$ and $\tilde{\mathbf{I}}_{i+1}$ are denoted as the prior and next video frame, respectively.

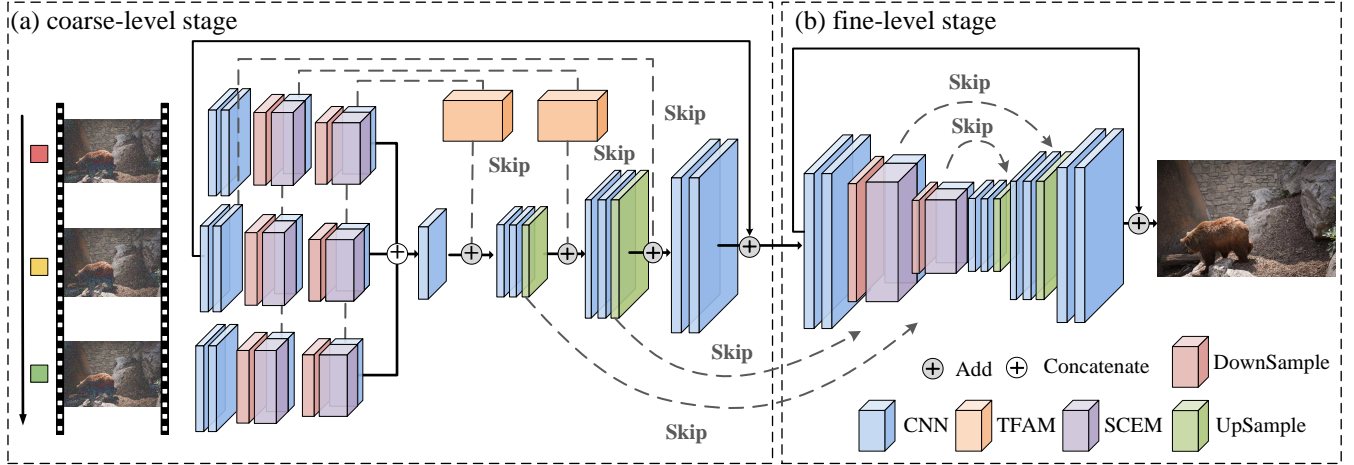


Figure 2: Overview of our proposed DSCT model. The *coarse-level stage* extracts the dynamic features from the neighbor frames, while the *fine-level stage* extracts the fine-grained static representations from the denoised results. Both stages are constructed in an encoder-decoder architecture. The encoder of each stage contains a Spatial-Channel Encoding Module to extract long-range spatial-channel information. The *Multi-scale Residual Structure* is introduced to maintain the multiple aspects information in different stage, and a Temporal Features Aggregation Module is adopted to summarize the dynamic representation.

Multi-frame Encoder Module. Firstly, we use two 3×3 convolution layers followed by BN [5] and ReLU [4] to extract initial features I^C from different frames:

$$I^C = \text{Conv}(\hat{\mathbf{I}}), \quad (1)$$

where $\text{Conv}(\cdot)$ means the convolution operation.

Then, the feature passed through two downsample operations, each followed by a Spatial-Channel Encoding Module and two 3×3 convolution layers. The features captured from Spatial-Channel Encoding module and CNN are combined as the output I^{SC} , which is formulated as:

$$I^{SC} = \text{SC}(X) + \text{Conv}(X), \quad (2)$$

where $\text{SC}(\cdot)$ is the function of Spatial-Channel Encoding Module, X denotes the feature after downsampling.

Finally, we obtain the low-level spatial features and high-level dynamic representation of three continuous frames and then fed them into the decoder to obtain the denoised results I' at the *coarse-level stage*.

Spatial-Channel Encoding Module. In a given video, different spatial resolution frames contain rich hierarchical representation, and more channels means more specific information. Therefore, we design a Spatial-Channel Encoding Module (SCEM) to model the long-range dependencies at both spatial position and channel. The details of the process is shown in Figure 3.

Given a feature $X \in \mathbb{R}^{C \times H \times W}$ as input for the Spatial-Channel Encoding Module, we split it by the patch size of $P \times P$, and then reshape the feature into size $\frac{HW}{P^2} \times P^2 \times C$, where $\frac{HW}{P^2}$ represents the total number of patches. Firstly, we feed the feature $X \in \mathbb{R}^{\frac{HW}{P^2} \times P^2 \times C}$ through a LayerNorm (LN) layer, and reshape it to $X \in \mathbb{R}^{\frac{HW}{P^2} \times C \times P^2}$.

Then we compute the self-attention (denoted as SA) for feature X , as the following:

$$\hat{X} = \text{SA}(\text{LN}(X)), \quad (3)$$

where $\text{LN}(\cdot)$ denotes the LayerNorm operator, and the size of the attention feature map through softmax is $C \times C$.

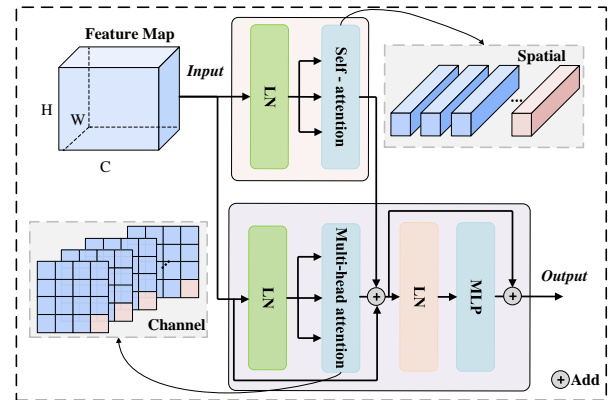


Figure 3: Illustration of the proposed Spatial-Channel Encoding Module, which explores global feature from both spatial and channel levels.

Meanwhile, multi-head self-attention layer (denoted as MSA) takes the feature $X \in \mathbb{R}^{\frac{HW}{P^2} \times P^2 \times C}$ as input, and then calculates the multi-head attention as:

$$\hat{X}^l = \text{MSA}(\text{LN}(X)), \quad (4)$$

where $\text{LN}(\cdot)$ denotes the LayerNorm operator, and the size of the attention feature map through softmax is $P^2 \times P^2$. In addition, a multi-layer perceptron (MLP) is also used for further feature transformation followed by one additional LN layer, which can be formulated as follows:

$$\mathbf{X} = \text{MLP} \left(\text{LN} \left(\hat{\mathbf{X}} + \hat{\mathbf{X}}^l \right) \right) + \mathbf{X}. \quad (5)$$

Finally, we reshape the features back to $\mathbf{X} \in \mathbb{R}^{C \times H \times W}$, and obtain the global features containing both spatial and channel information. **Decoder Module.** We pass the output of the Multi-frame Encoder Module through a 1×1 convolution layer, which aims to control the number of the channels as the following:

$$\mathbf{I}^F = \text{Conv}(\mathbf{I}_{i-1}^{ME}, \mathbf{I}_i^{ME}, \mathbf{I}_{i+1}^{ME}), \quad (6)$$

where $\mathbf{I}_{i-1}^{ME}, \mathbf{I}_i^{ME}, \mathbf{I}_{i+1}^{ME}$ denote the output of the Multi-frame Encoding Module. The decoder module exploits the small-scale convolution filters to capture fine-grained cues, and the Pixelshuffle [15] upsampling operation to recover the spatial and channel structure. In the module, we denote two 3×3 convolutional filters and a upsampling operation as an upsampling layer. Following the upsampling layer, two convolution layers are used to smooth and restore the upsampling result as the clean version of the input $\mathbf{I}' \in \mathbb{R}^{H \times W \times C}$.

3.2 Fine-Level Stage

Since the proposed *coarse-level stage* aims to extract dynamic feature from video neighborhood frames to obtain the coarse-grained results, we further use the *fine-level stage* to extract the static feature from the output of *coarse-level stage* to achieve the fine-grained denoising result.

During the *fine-level stage*, we adopt the similar architecture as the *coarse-level stage*, which includes Spatial-Channel Transformer to extract global and local features. Compared to the *coarse-level stage*, the encoder of *fine-level stage* accepts the output from the decoder of the *coarse-level stage*, so there is only one branch in the encoder and the decoder only uses a simple skip-connection operation here.

We takes the output $\mathbf{I}' \in \mathbb{R}^{H \times W \times C}$ of the previous stage as input, and the restored clean video frames $\hat{\mathbf{I}} \in \mathbb{R}^{H \times W \times C}$ can be obtained as the following:

$$\hat{\mathbf{I}} = H_{Fl}(\mathbf{I}'), \quad (7)$$

where $H_{Fl}(\cdot)$ denotes the functions of the encoder and decoder at the *fine-level stage*.

3.3 Multi-Scale Residual Structure

We design a *multi-scale residual structure* to preserve multiple aspects of information during different stages, which contains three different skip operations as follows:

(1) **Coarse-level stage:** We introduce the skip-connections between decoder and encoder at the *coarse-level stage*, which aims to retain the temporal information from different frames. Instead of using a simple concatenate or mean operation to aggregate temporal information, the temporal information can be captured by the proposed *Temporal Features Aggregation Module* (TFAM), by

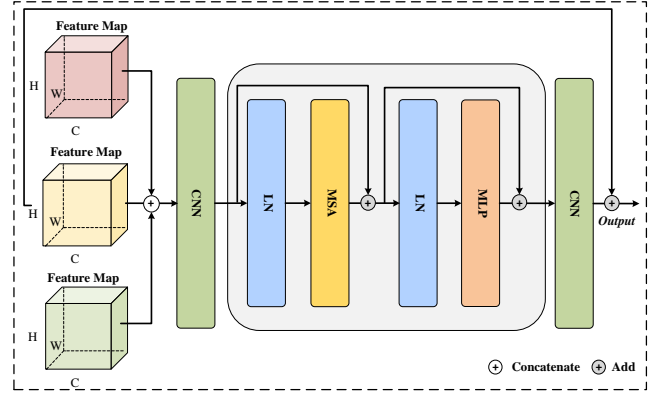


Figure 4: Illustration of the Temporal Features Aggregation Module, which exploit the self-attention mechanism to incorporate the global context for different video frames.

providing additional information for reconstructing target frames and make the restoration process robust, as shown in Figure 4.

TFAM receives the feature \mathbf{I}^{SC} as input, and aggregate the features with temporal factors. We first pass the adjacent frames feature $\mathbf{I}_{i-1}^{SC}, \mathbf{I}_i^{SC}, \mathbf{I}_{i+1}^{SC}$ through a 3×3 convolution layer, which aims to extract local features and expand the perception field of input to fit the subsequent transformer.

Then, the features \mathbf{I}^C from the CNN are fed into a MSA layer [37] to obtain the global context information, where the MSA layer is followed by one MLP layer and one LayerNorm (LN) layer.

$$\begin{aligned} \mathbf{I}^C &= \text{MSA}(\text{LN}(\mathbf{I}^C)) + \mathbf{I}^C; \\ \mathbf{I}^C &= \text{MLP}(\text{LN}(\mathbf{I}^C)) + \mathbf{I}^C. \end{aligned} \quad (8)$$

Finally, the size of the channels is controlled by a 3×3 convolutional layer.

And we use a residual operation on the input features of the intermediate frames and the output of the TFAM. Finally we get the aggregated temporal information \mathbf{I}^{TFAM} .

(2) **Between the coarse-level stage and the fine-level stage:** We introduce the skip-connections to bridge the *coarse-level stage* decoder and the *fine-level stage* encoder. By utilizing such skip-connections, we can introduce intermediate-level context information from the *fine-level stage* encoder to make the network gain more knowledge and thus beneficial to denoise. On the other hand, it can avoid the gradient-vanishing due to the deeper network, and ensure the network can back-propagate the gradient properly during the training.

(3) **Fine-level stage:** We introduced the skip-connections between decoder and encoder at this stage, in order to preserve low-level spatial features and high-level semantic context.

3.4 Loss Function

Finally, the proposed whole network can be trained in an end-to-end manner with the L_2 loss, formulated as the following:

$$\mathcal{L} = \frac{1}{2N} \sum_{i=1}^N \|\hat{\mathbf{I}}_i - \mathbf{I}_i\|^2, \quad (9)$$

where \hat{I}_i and I_i indicate the denoising frame results and ground truth clean frame, respectively, and N is the number of the training data.

4 EXPERIMENTS

To verify the effectiveness of our proposed method, we conduct extensive experiments on four widely-adopted datasets, *i.e.*, Davis [10], Set8 [2], Vimeo90k [22] and Raw Videos [28]. Note that we train our model on Davis, then test our model on Davis-test, Set8, Vimeo90k-test. To evaluate the generalization performance, we test our model on the real dynamic Raw videos dataset [28].

4.1 Datasets and Settings

Davis [10] is a high quality and resolution video segmentation dataset. It contains both 480p and 1080p resolution densely annotated videos, and we chose 480p resolution data for training and testing. In practice, we select 90 video sequences as the training set and another 30 sequences for test.

Set8 [2] includes 8 video sequences of size 960×540, of which four sequence are collected from Derf’s Test Media collection and another four from the GoPro camera.

Vimeo90k [22] is a video dataset covering a variety of real-world scenes and actions, which consists of 89,000 videos of size 256×448. Vimeo90k-test is used for evaluation including 7824 sequences and each sequence contains 7 frames.

Raw videos [28] is a real noisy video dataset which has a total of 11 different videos of indoor scenes, and each video consists of 7 frames. The different scenes were captured using cameras with five different ISO levels from 1600 to 25600, leading to different levels of noises in videos.

Metrics. We use two quantitative measure to evaluate the performance: Peak Signal-to-Noise Ratio (PSNR) and Spatio-Temporal Reduced Reference Entropic Differences (ST-RRED) [1].

Compared Methods. To evaluate the effectiveness of the proposed DSCT, we compare our model with the state-of-the-art video denoising and image denoising methods. The video denoising methods include V-BM4D [3], TOFlow [22], VNLB [24], VNLnet [25], FastDVDnet [2], DVDnet [21], UDVD[27], RViDeNet [28], PaCNet [11], and DIDN [16]. Image denoising methods include DnCNN [9] and NBNNet [26], which take each frame of the video as input to the model during training and evaluation.

4.2 Implementation Details

We implement our DSCT with PyTorch [8] and GeForce RTX 2080 Ti GPU. We train our model with Adam optimizer[36] with $\beta_1 = 0.9$, $\beta_2 = 0.999$ and 100 epochs, and the initial value of the learning rate is set as 0.001, with the learning rate decays by a factor of 10 at the 50,60,80 epochs in turn. The batch size is set to 64. The training frames are cropped into 96×96 RGB patches and the contiguous frames are cropped at the same location. During training, we augment the training data by random horizontal flips and vertical flips with random rotation scale factors of 90°, 180° and 270°. The patch size and head size are set to 4×4 and 4. Following the same setting in [2], each sequence is limited to a maximum of 85 frames during the evaluation stage.

4.3 Evaluation

Results on Gaussian noise. We evaluate the denoising performance of our proposed model on different nature video datasets. During training, we train the model with the Davis training set by adding additive white Gaussian noise (AWGN) of $\sigma \in [5, 50]$ to the clean video sequence. During testing, we add Gaussian noise with five representative standard deviations $\sigma = 10, 20, 30, 40,$ and 50 for the test set. Table 1 shows the evaluation results in terms of PSNR and ST-RRED on the Davis, Set8 and Vimeo90k dataset. We can find our proposed DSCT outperforms the all the state-of-the-art video/image denoising methods under different noise w.r.t PSNR, and achieves competitive results w.r.t ST-RRED on Davis and Set8 dataset. We explain the improved performance as the following reasons: firstly, the *coarse-level stage* can fuse the effective information of the noised frame with its neighbors, and the *fine-level stage* can fully exploit the hidden information in the coarse-level denoising results to generate the more clean version than the coarse-level one; secondly, our method inherits the advantage of the transformer and the CNN, which can effectively model the long-rang dependency and local perception at the same time.

Furthermore, we conducted experiments on the Vimeo90k dataset to verify the generality of our approach. We show the evaluation results on Table 1 by comparing our proposed method with DnCNN [9], V-BM4D [3], TOFlow [22], and FastDVDnet [2]. We can observe that our method can obtain the best results in terms of PSNR. Meanwhile, with the increasing of noise standard, our model can still obtain satisfied results. For example, the PSNR of our proposed method can reach to 33.46 at the noise standard of 50, demonstrating our method has better generality than other competitors. However, FastDVDnet [2] achieves slightly better results w.r.t ST-RRED than our method, because they utilize more reference frames than we used to recovery the current frame.

Regarding the qualitative results, we show a few of visual results on Davis and Set8 datasets at $\sigma = 50$ in Figure 5 and Figure 6, respectively. We observe that our method recovers more fine-grained and clearer details in a frame than other methods, especially the visual appearance of the bud part of the tree trunk, the nose of the face, and the bumpy of the snow traces. While the videos restored by another methods have more blurry background. The better visualization results indicate that we combine local and global information from video frames for denoising can generate natural and smooth visual content. Besides, it demonstrates that our proposed Multi-scales Residual Structure can reconstruct enough details. Furthermore, the visual results of the dual-stage are clearer than the results only with the *coarse-level stage* or the *fine-level stage*, which intuitively indicate that our proposed coarse-to-fine strategy is very useful.

Results on real noise. To verify the effectiveness of our method with real noise, we further evaluate the proposed DSCT method on Raw Videos dataset. During the training and evaluation, we adopt the same training data and testing data followed [27], and optimize our model under each specific ISO setting. We present the results on Raw videos dataset under ISO level setting 1600 in Figure 7. We can observe that our method outperforms the previous methods, such as DIDN [16], RViDeNet[28] and UDVD [27], indicating our method can capture more effective global contextual dependencies to greatly

Table 1: PSNR/ST-RRED comparison of the state-of-the-art denoising methods on Davis, Set8 and Vimeo90k datasets. The best performance is highlighted in bold.

Dataset	Methods	10	20	30	40	50
		PSNR/ST-RRED	PSNR/ST-RRED	PSNR/ST-RRED	PSNR/ST-RRED	PSNR/ST-RRED
Davis	DnCNN [9]	38.28/3.26	34.74/11.75	32.74/24.85	31.34/42.04	30.27/63.50
	NBNet [26]	32.83/6.86	29.94/23.44	28.22/48.20	26.91/80.13	25.80/119.99
	V-BM4D [3]	37.58/4.26	33.88/11.02	31.65/21.91	30.05/36.60	28.80/54.82
	VNLB [24]	38.85/3.22	35.68/6.77	33.73/ 12.08	32.32/19.33	31.13/28.21
	VNLnet [25]	35.83/2.81	34.49/ 6.11	-	32.32/18.63	31.43/28.67
	DVDnet [21]	38.13/4.28	35.70/7.54	34.08/12.19	32.86/ 18.16	31.85/ 25.63
	FastDVDnet [2]	38.71/3.49	35.77/7.46	34.04/13.08	32.82/20.93	31.86/28.89
	PaCNet [11]	39.97/ -	36.82/ -	34.79/ -	33.34/ -	32.20/ -
	UDVD [27]	-	-	33.92/ -	32.68/ -	31.70/ -
	DSCT (Ours)	40.19/2.30	36.96/6.77	35.08/13.09	33.74/21.23	32.69/31.06
Set8	DnCNN [9]	36.22/2.72	32.69/10.23	30.72/22.70	29.36/39.74	28.32/60.41
	NBNet [26]	31.15/6.38	28.17/22.40	26.47/45.87	25.24/75.06	24.26/108.53
	V-BM4D [3]	36.05/3.87	32.19/9.89	30.00/19.58	28.48/32.82	27.33/49.20
	VNLB [24]	37.26/2.86	33.72/6.28	31.74/ 11.53	30.39/18.57	29.24/27.39
	VNLnet [25]	37.10/3.43	33.88/6.88	-	30.55/19.71	29.47/29.78
	DVDnet [21]	36.08/4.16	33.49/7.54	31.79/12.61	30.55/19.05	29.56/27.97
	FastDVDnet [2]	36.44/3.00	33.43/6.65	36.18/11.85	30.64/ 18.45	29.53/ 26.75
	PaCNet [11]	37.06/ -	33.94/ -	32.05/ -	30.70/ -	29.66/ -
	UDVD [27]	-	-	32.01/ -	30.92/ -	29.89/ -
	DSCT (Ours)	37.02/ 2.06	33.96/6.26	32.16/12.12	30.91/19.68	29.93/28.83
Vimeo90k	DnCNN [9]	39.41/4.83	36.08/17.41	34.06/36.72	32.60/62.10	31.45/92.63
	V-BM4D [3]	40.23/3.93	36.22/11.60	33.71/22.87	31.86/37.46	30.40/55.17
	TOFlow [22]	31.45/30.62	34.43/27.43	31.76/28.33	27.87/32.84	24.92/41.32
	FastDVDNet [2]	38.87/ 2.93	36.15/ 8.13	34.40/ 15.15	33.09/ 24.02	32.05/ 34.62
	DSCT (Ours)	40.77/3.11	37.81/8.65	35.95/16.32	34.56/25.99	33.46/37.73



Figure 5: Denoising visualized results with Gaussian noise level $\sigma = 50$ on Davis dataset.

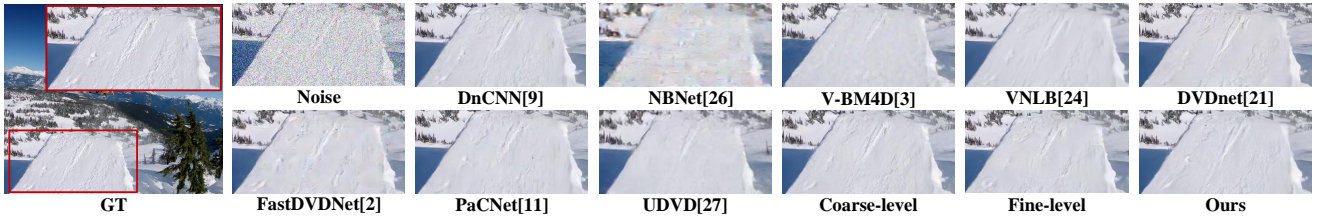


Figure 6: Denoising visualized results with Gaussian noise level $\sigma = 50$ on Set8 dataset.

beneficial the denoising results. More experimental results and details will be presented in our supplementary materials.

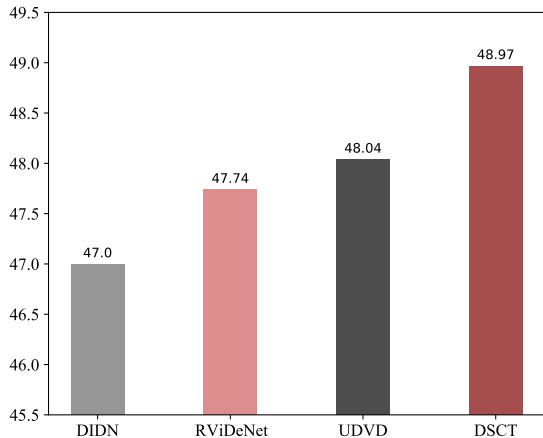


Figure 7: PSNR comparison with state-of-the-art denoising methods under 1600 ISO settings.

4.4 Ablation Study

In this section, we conduct the ablation studies to examine the impact of different components in our approach on Davis and Set8 datasets with Gaussian noise standard $\sigma=30$.

Impact of different stage. We explore the impact of the *coarse-level stage* and the *fine-level stage*. One is only has a coarse stage and the other only has a fine stage. The results are shown in the Table 2. As listed in the table, the results of only the *coarse-level stage* or the *fine-level stage* are not satisfied, while the results of both stages achieves the best performance demonstrating the coarse-to-fine strategy is rewarding for the video denoising.

Effect of the Spatial-Channel Transformer. We explore the effectiveness of the proposed Spatial-Channel Transformer in different modules. The ablation experimental results are shown in Table 3, which ST denotes swin transformer and SCEM denotes the proposed Spatial-Channel Encoding Module. We adopt the CNN architecture as the *base* model by only removing all transformer part and the Temporal Features Aggregation Module (TFAM) part. Following the base model, we progressively add different parts: firstly, we add a normal Swin transformer layer [37] as *base+ST* model, and then we replace it with our proposed Spatial-Channel Encoding module denoted as *base+SCEM* model. In addition, we add Temporal Features Aggregation Module (TFAM) to each of the above two models to obtain *base+ST+TFAM* model and our DSCT model. As shown in the table, after incorporating the transformer, the PSNR performance can be improved from 33.69 to 34.32 on Davis dataset, which verifies the effectiveness of the modelling long-range dependency. When Spatial-Channel Encoding Module is incorporated, the PSNR performance can be improved from 31.66 to 31.94 on Set8 dataset, showing the effectiveness of capturing long-range information from both spatial and channel.

Impact of the Multi-scale Residual Structure. We conduct ablative experiments to verify the effectiveness of each skip-connection operation in our model, by removing another skip-connection operations separately. The experimental results are shown in the Table 4 under the Gaussian noise with standard $\sigma=30$. We denote

Table 2: PSNR/ST-RRED comparison among Coarse-level stage and Fine-level stage.

Method	Coarse-level stage	Fine-level stage	Ours
Davis	34.91/13.97	33.79/23.34	35.08/13.09
Set8	32.07/13.03	31.35/21.68	32.16/12.12

Table 3: Ablation study on different modules. Test on the Davis and Set8 dataset with a noise standard of 30. ST denote SwinTransformer, SCEM denote Spatial-Channel Encoding Module, TFAM denote Temporal Features Aggregation Module.

Method	ST	SCEM	TFAM	PSNR/ST-RRED	
				Davis	Set8
base				33.69/15.60	31.24/14.36
base+ST	✓			34.32/16.46	31.66/15.43
base+ST+TFAM	✓		✓	34.80/14.11	31.99/13.15
base+SCEM		✓		34.75/14.21	31.94/12.99
Ours		✓	✓	35.08/13.09	32.16/12.12

Table 4: PSNR/ST-RRED comparison among different skip-connection operation, where *DF-Skip* denotes the model without F-skip operation, *DCF-Skip* denotes the model without CF-skip operation, and *DTFAM* denotes the model without TFAM.

Method	DF-Skip	DCF-Skip	DTFAM	Ours
Davis	35.01/13.57	34.15/22.10	34.16/14.51	35.08/13.09
Set8	32.16/12.20	31.58/20.82	31.94/12.99	32.16/12.12

the skip-connection operation in *fine-level stage* as *F-Skip*, the skip-connection operation between *coarse-level stage* and *fine-level stage* as *CF-Skip*, and the skip-connection operation in *coarse-level stage* as *TFAM*. From Table 4, we can observe that performance degrades when each skip-connection operation is removed, so our proposed three skip-connection operation is an integral part to bring significant performance improvement.

In addition, we have validated different methods for aggregating multi-frame temporal information, such as fusing features using the mean method, Convolution operation, and our proposed Temporal Features Aggregation Module (TFAM). The experimental results are shown in Table 5, and we can see that our proposed TFAM beats another methods across both metrics, *i.e.*, PSNR and ST-RRED. It demonstrates that our proposed TFAM can fully integrate the temporal features of different frames compared with the simple mean or Conv operations.

Visualization results of different modules. To further verify the validity of each module, we visualized the features output of *Spatial-Channel Encoding module* (SCEM) and *Temporal Features Aggregation Module* (TFAM) from the first part of the *coarse-level stage*. It can be seen from the Figure 8 that TFAM can pay more attentions to both background and boundary detailed information, and SCEM focuses on the spatial detailed information.

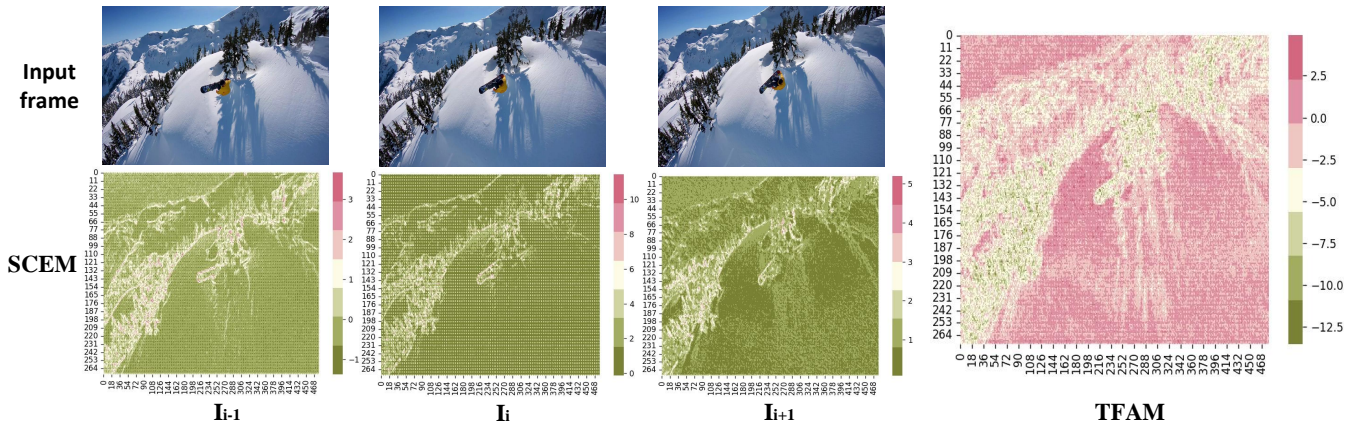


Figure 8: Some visualizations of DSCT. We show the features of the consecutive input frames after the first pass through Spatial-Channel Encoding module (SCEM) and Temporal Features Aggregation Module (TFAM) of the coarse-level stage, respectively. We find that the SCEM gives higher attention to detail information compared to background information. And the TFAM gives more attention to the background information than the detailed information.

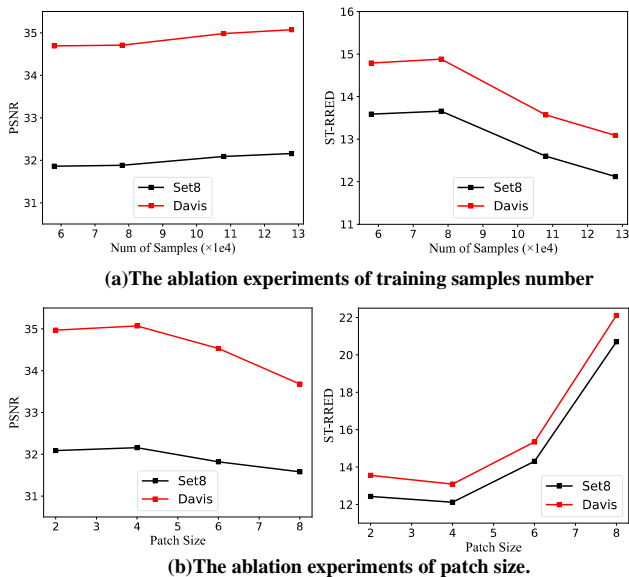


Figure 9: Ablation study on the training samples number and the patch size.

Table 5: PSNR/ST-RRED comparison among different aggregation methods, i.e., Mean, Conv operation and Temporal Features Aggregation module.

Method	Mean	Conv	TFAM (Ours)
Davis	34.14/22.02	34.52/15.93	35.08/13.09
Set8	31.55/20.86	31.75/15.12	32.16/12.12

The number of training samples and patch size. We conduct ablation experiments w.r.t the number of training samples and the patch size of the transformer, and Figure 9 shows the corresponding experimental results. Figure9 (a) shows the experimental results of

various numbers of training samples. We increase the number of training samples sequentially from 58,000 to 128,000 in a span of 20,000. As expected, the performance of our model increases along with the number of training samples. In addition, from Figure9 (b), we can see that the best performance is achieved when we set the patch size as 4×4 , demonstrating the too large patch size is suitable for visual recognition instead of video denoising, e.g., VIT [32] set patch size to 16×16 for classification. While the too small patch size is not fit to our task because and the interaction between pixel points ignore the corresponding texture information. Therefore, the patch size of 4×4 ensures the best results are achieved by focusing on the location information of the noise and texture details.

5 CONCLUSION

In this paper, we propose a novel Dual-stage Spatial-Channel Transformer (DSCT), which uses the progressive coarse-to-fine strategy for video denoising. We design a Spatial-channel Transformer to simultaneously capture improved spatio-temporal features, and a Spatial-Channel Encoding Module to build long-range spatial-channel information. In addition, a multi-scale residual structure is introduced to reserve the video detail information and enhance the representation on each level. Extensive experiments on four public benchmarks demonstrate the effectiveness and superiority of the proposed DSCT.

REFERENCES

- [1] R. Soundararajan and A. Bovik, "Video quality assessment by reduced reference spatio-temporal entropic differencing," *IEEE Transactions on Circuits and Systems for Video Technology*, vol. 23, no. 4, pp. 684–694, 2013.
- [2] M. Tassano, J. Delon, and T. Veit, "Fastdvdnet: Towards real-time deep video denoising without flow estimation," in *2020 IEEE/CVF Conference on Computer Vision and Pattern Recognition (CVPR)*, 2020, pp. 1351–1360.
- [3] M. Maggioni, G. Boracchi, A. Foi, and K. Egiazarian, "Video denoising, deblocking, and enhancement through separable 4-d nonlocal spatiotemporal transforms," *IEEE Transactions on Image Processing*, vol. 21, no. 9, pp. 3952–3966, 2012.
- [4] X. Glorot, A. Bordes, and Y. Bengio, "Deep sparse rectifier neural networks," in *Proceedings of the fourteenth international conference on artificial intelligence and statistics*. Fort Lauderdale, USA: JMLR Workshop and Conference Proceedings, 2011, pp. 315–323.
- [5] S. Ioffe and C. Szegedy, "Batch normalization: Accelerating deep network training by reducing internal covariate shift," in *International conference on machine*

- learning. Lille, France: JMLR.org, 2015, pp. 448–456.
- [6] P. Ramachandran, N. Parmar, A. Vaswani, I. Bello, A. Levskaya, and J. Shlens, “Stand-alone self-attention in vision models,” *Advances in Neural Information Processing Systems*, vol. 32, 2019.
 - [7] H. Cao, Y. Wang, J. Chen, D. Jiang, X. Zhang, Q. Tian, and M. Wang, “Swin-UNET: Unet-like pure transformer for medical image segmentation,” *arXiv*, vol. abs/2105.05537, 2021.
 - [8] A. Paszke, S. Gross, F. Massa, A. Lerer, J. Bradbury, G. Chanan, T. Killeen, Z. Lin, N. Gimelshein, L. Antiga *et al.*, “Pytorch: An imperative style, high-performance deep learning library,” *Advances in neural information processing systems*, vol. 32, pp. 8026–8037, 2019.
 - [9] K. Zhang, W. Zuo, Y. Chen, D. Meng, and L. Zhang, “Beyond a gaussian denoiser: Residual learning of deep cnn for image denoising,” *IEEE Transactions on Image Processing*, vol. 26, no. 7, pp. 3142–3155, 2017.
 - [10] A. Khoreva, A. Rohrbach, and B. Schiele, “Video object segmentation with language referring expressions,” in *Asian Conference on Computer Vision*. Mounts Bay Road, Perth: Springer, 2018, pp. 123–141.
 - [11] G. Vaksman, M. Elad, and P. Milanfar, “Patch craft: Video denoising by deep modeling and patch matching,” in *Proceedings of the IEEE/CVF International Conference on Computer Vision (ICCV)*, October 2021, pp. 2137–2146.
 - [12] S. Laine, T. Karras, J. Lehtinen, and T. Aila, *High-Quality Self-Supervised Deep Image Denoising*. Red Hook, NY, USA: Curran Associates Inc., 2019.
 - [13] S. W. Zamir, A. Arora, S. Khan, M. Hayat, F. S. Khan, M.-H. Yang, and L. Shao, “Multi-stage progressive image restoration,” in *2021 IEEE/CVF Conference on Computer Vision and Pattern Recognition (CVPR)*, 2021, pp. 14 816–14 826.
 - [14] X. Li, Y. Hou, P. Wang, Z. Gao, M. Xu, and W. Li, “Treat: Transformer-based rgb-d egocentric action recognition,” *IEEE Transactions on Cognitive and Developmental Systems*, vol. 14, no. 1, pp. 246–252, 2022.
 - [15] W. Shi, J. Caballero, F. Huszár, J. Totz, A. P. Aitken, R. Bishop, D. Rueckert, and Z. Wang, “Real-time single image and video super-resolution using an efficient sub-pixel convolutional neural network,” in *2016 IEEE Conference on Computer Vision and Pattern Recognition (CVPR)*, 2016, pp. 1874–1883.
 - [16] S. Yu, B. Park, and J. Jeong, “Deep iterative down-up cnn for image denoising,” in *2019 IEEE/CVF Conference on Computer Vision and Pattern Recognition Workshops (CVPRW)*, 2019, pp. 2095–2103.
 - [17] Z. Wang, X. Cun, J. Bao, and J. Liu, “Uformer: A general u-shaped transformer for image restoration,” *arXiv*, vol. abs/2106.03106, 2021.
 - [18] K. Dabov, A. Foi, V. Katkovnik, and K. Egiazarian, “Image denoising by sparse 3-d transform-domain collaborative filtering,” *IEEE Transactions on image processing*, vol. 16, no. 8, pp. 2080–2095, 2007.
 - [19] O. Ronneberger, P. Fischer, and T. Brox, “U-net: Convolutional networks for biomedical image segmentation,” in *International Conference on Medical image computing and computer-assisted intervention*. Springer, 2015, pp. 234–241.
 - [20] H. Touvron, M. Cord, M. Douze, F. Massa, A. Sablayrolles, and H. Jégou, “Training data-efficient image transformers & distillation through attention,” in *International Conference on Machine Learning*, vol. 139. online: PMLR, 2021, pp. 10 347–10 357.
 - [21] M. Tassano, J. Delon, and T. Veit, “Dvdnet: A fast network for deep video denoising,” in *2019 IEEE International Conference on Image Processing (ICIP)*, 2019, pp. 1805–1809.
 - [22] T. Xue, B. Chen, J. Wu, D. Wei, and W. T. Freeman, “Video enhancement with task-oriented flow,” *International Journal of Computer Vision (IJCV)*, vol. 127, no. 8, pp. 1106–1125, 2019.
 - [23] X. Chen, L. Song, and X. Yang, “Deep rnns for video denoising,” in *Applications of Digital Image Processing XXXIX*, vol. 9971. San Diego, California: SPIE, September 2016, pp. 573–582. [Online]. Available: <https://www.spiedigitallibrary.org/conference-proceedings-of-spie/9971/99711T/Deep-RNNs-for-video-denoising/10.1117/12.2239260.full>
 - [24] P. Arias and J.-M. Morel, “Video denoising via empirical bayesian estimation of space-time patches,” *Journal of Mathematical Imaging and Vision*, vol. 60, no. 1, pp. 70–93, 2018.
 - [25] A. Davy, T. Ehret, G. Facciolo, J. Morel, and P. Arias, “Non-local video denoising by cnn,” *ArXiv*, vol. abs/1811.12758, 2018.
 - [26] S. Cheng, Y. Wang, H. Huang, D. Liu, H. Fan, and S. Liu, “Nbnnet: Noise basis learning for image denoising with subspace projection,” in *2021 IEEE/CVF Conference on Computer Vision and Pattern Recognition (CVPR)*. online: IEEE, 2021, pp. 4894–4904.
 - [27] D. Y. Sheth, S. Mohan, J. L. Vincent, R. Manzorro, P. A. Crozier, M. M. Khapra, E. P. Simoncelli, and C. Fernandez-Granda, “Unsupervised deep video denoising,” in *Proceedings of the IEEE/CVF International Conference on Computer Vision (ICCV)*, October 2021, pp. 1759–1768.
 - [28] H. Yue, C. Cao, L. Liao, R. Chu, and J. Yang, “Supervised raw video denoising with a benchmark dataset on dynamic scenes,” in *Proceedings of the IEEE/CVF Conference on Computer Vision and Pattern Recognition (CVPR)*, June 2020, pp. 2298–2307.
 - [29] N. Carion, F. Massa, G. Synnaeve, N. Usunier, A. Kirillov, and S. Zagoruyko, “End-to-end object detection with transformers,” in *European Conference on Computer Vision*, 2020, pp. 213–229.
 - [30] H. Chen, Y. Wang, T. Guo, C. Xu, Y. Deng, Z. Liu, S. Ma, C. Xu, C. Xu, and W. Gao, “Pre-trained image processing transformer,” in *CVPR*, 2021, p. 1229.
 - [31] A. Vaswani, N. Shazeer, N. Parmar, J. Uszkoreit, L. Jones, A. N. Gomez, L. Kaiser, and I. Polosukhin, “Attention is all you need,” in *Advances in neural information processing systems*, 2017, pp. 6000–6010.
 - [32] A. Kolesnikov, A. Dosovitskiy, D. Weissenborn, G. Heigold, J. Uszkoreit, L. Beyer, M. Minderer, M. Dehghani, N. Houlsby, S. Gelly *et al.*, “An image is worth 16x16 words: Transformers for image recognition at scale,” in *International Conference on Learning Representations*, 2021.
 - [33] M. Claus and J. van Gemert, “Videnn: Deep blind video denoising,” in *Proceedings of the IEEE/CVF Conference on Computer Vision and Pattern Recognition Workshops*, 2019, pp. 1843–1852.
 - [34] C. Wang, S. K. Zhou, and Z.-Q. Cheng, “First image then video: A two-stage network for spatiotemporal video denoising,” *ArXiv*, vol. abs/2001.00346, 2020.
 - [35] X. Tao, H. Gao, X. Shen, J. Wang, and J. Jia, “Scale-recurrent network for deep image deblurring,” in *2018 IEEE/CVF Conference on Computer Vision and Pattern Recognition*, 2018, pp. 8174–8182.
 - [36] D. P. Kingma and J. Ba, “Adam: A method for stochastic optimization,” *Computer Science*, vol. abs/1412.6980, 2014.
 - [37] Z. Liu, Y. Lin, Y. Cao, H. Hu, Y. Wei, Z. Zhang, S. Lin, and B. Guo, “Swin transformer: Hierarchical vision transformer using shifted windows,” in *2021 IEEE/CVF International Conference on Computer Vision (ICCV)*. IEEE, 2021, pp. 9992–10 002.

In the following, we first show the ablation experimental results about the learning rate. Then, we present the details of the visual effect on the Vimeo90k dataset, and show more visualization results of the Spatial-Channel Encoding module (SCEM) and Temporal Features Aggregation Module (TFAM). Finally, we illustrate a few of denoising results on real noise video data.

1 ABLATION STUDY

Impact of the learning rate. Different learning rates have various effects on the performance of our proposed model. Here we evaluate our model under different learning rates (0.0008, 0.0009, 0.0010 and 0.0011) on Set8 and Davis datasets with Gaussian noise standard $\sigma = 30$. The experimental results are shown in Figure 1. We can observe that our proposed method obtains the best performance when the learning rate is set as 0.001. Moreover, we also find that our method exhibits the stable performance under different learning rate, demonstrating the robustness of our proposed model.

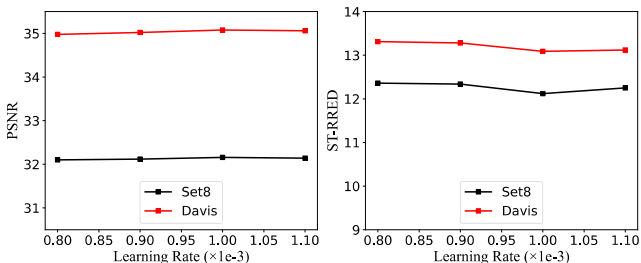


Figure 1: Ablation study on different learning rates. Test on the Davis and Set8 dataset with a noise standard of 30.

2 VISUALIZATION RESULTS

Visualization results on Vimeo90k. We present more visualization results on the Vimeo90k dataset here. Figure 2 and Figure 3 shows the visualization results by comparing our proposed method with DnCNN [4], V-BM4D [3], TOFlow [2], FastDVDnet [1] on the Vimeo90k dataset with the Gaussian noise under standard deviation $\sigma = 50$.

According to the visualization results, our proposed model can recover clearer details for nail cap and hand details than other state-of-the-art methods. The reasons stem from: firstly, we use a coarse-to-fine strategy to progressively implement coarse-grained to fine-grained denoising; secondly, our method inherits the advantages of both CNN and transformer in extracting local features and modeling long-range information compared to other methods; lastly, we preserve the important detailed information of the video during denoising.

Visualization result of SCEM and TFAM. In the main paper, we show the results of the consecutive input frames after the first pass during the coarse-level stage through the Spatial-Channel Encoding module (SCEM) and the Temporal Features Aggregation Module (TFAM), and then here we show the output results of second pass through SCME and TFAM. These results are shown in

Figure 4, and we show the results on two different consecutive sequences from Davis (top) and Set8 (bottom) datasets. According to the visualization results, we can observe that the output features through the first pass contain the low-level spatial information of the video frames, and the output features after the second pass contain the high-level semantic context of the video frames. Furthermore, we observe that the SCEM focuses on extracting more detailed spatial information, while TFAM mainly focuses on capturing the background information.

3 DENOISING RESULTS ON REAL NOISE

As discussed in the main paper, we adopt the same training data and testing data followed [7] during the training and evaluation phase, and optimize our model under each specific ISO setting. We compare our method to previous state-of-the-art methods including DIDN [5], RViDeNet[6] and UDVD [7]. Among them, DIDN is a specific real-image denoising method. UDVD can directly optimize the denoising model on the Raw videos dataset. RViDeNet is pre-trained on synthetic data and then fine-tuned on the Raw video dataset.

We present the results in Table 1, and we can see that our proposed method obtains better performance on the Raw Videos dataset than another methods under different ISO level noisy types.

Table 1: PSNR comparison with our proposed method and other state-of-the-art denoising methods on Raw videos dataset. Different ISO represent various levels of noises.

ISO	1600	3200	6400	12800	25600
DIDN [5]	47.00	45.02	43.08	40.58	40.56
RViDeNet [6]	47.74	45.91	43.85	41.20	41.27
UDVD [7]	48.04	46.24	44.70	42.19	42.11
Ours	48.97	47.11	45.61	43.04	43.01

In order to intuitively observe the effectiveness of our method, we further show more visualization results on the Raw videos dataset under ISO level setting 25,600 in Figure 5. The results show that our proposed method eliminate the noise yet retaining the essential visual content, achieving better denoising results.

REFERENCES

- [1] M. Tassano, J. Delon, and T. Veit, "Fastdvdnet: Towards real-time deep video denoising without flow estimation," in *2020 IEEE/CVF Conference on Computer Vision and Pattern Recognition (CVPR)*, 2020, pp. 1351–1360.
- [2] T. Xue, B. Chen, J. Wu, D. Wei, and W. T. Freeman, "Video enhancement with task-oriented flow," *International Journal of Computer Vision (IJCV)*, vol. 127, no. 8, pp. 1106–1125, 2019.
- [3] M. Maggioni, G. Boracchi, A. Foi, and K. Egiazarian, "Video denoising, deblocking, and enhancement through separable 4-d nonlocal spatiotemporal transforms," *IEEE Transactions on Image Processing*, vol. 21, no. 9, pp. 3952–3966, 2012.
- [4] K. Zhang, W. Zuo, Y. Chen, D. Meng, and L. Zhang, "Beyond a gaussian denoiser: Residual learning of deep cnn for image denoising," *IEEE Transactions on Image Processing*, vol. 26, no. 7, pp. 3142–3155, 2017.
- [5] S. Yu, B. Park, and J. Jeong, "Deep iterative down-up cnn for image denoising," in *2019 IEEE/CVF Conference on Computer Vision and Pattern Recognition Workshops (CVPRW)*, 2019, pp. 2095–2103.

[6] H. Yue, C. Cao, L. Liao, R. Chu, and J. Yang, "Supervised raw video denoising with a benchmark dataset on dynamic scenes," in *Proceedings of the IEEE/CVF Conference on Computer Vision and Pattern Recognition (CVPR)*, June 2020, pp. 2298–2307.

[7] D. Y. Sheth, S. Mohan, J. L. Vincent, R. Manzorro, P. A. Crozier, M. M. Khapra, E. P. Simoncelli, and C. Fernandez-Granda, "Unsupervised deep video denoising," in *Proceedings of the IEEE/CVF International Conference on Computer Vision (ICCV)*, October 2021, pp. 1759–1768.

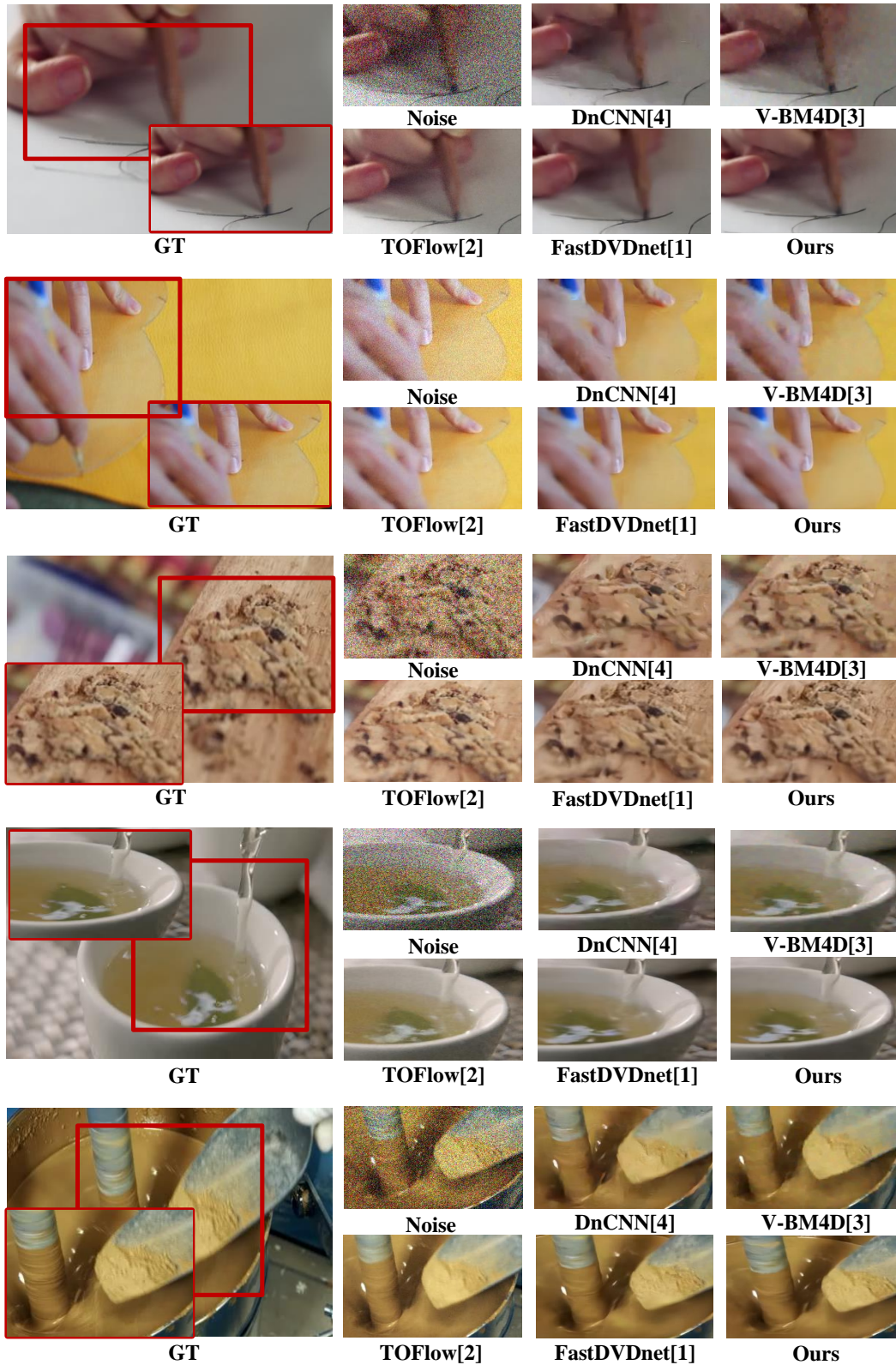


Figure 2: Denoising visualized results with Gaussian noise level $\sigma = 50$ on Vimeo90k dataset of the proposed DSCT and other state-of-the-art methods. From top to bottom shows different frames in a given video.

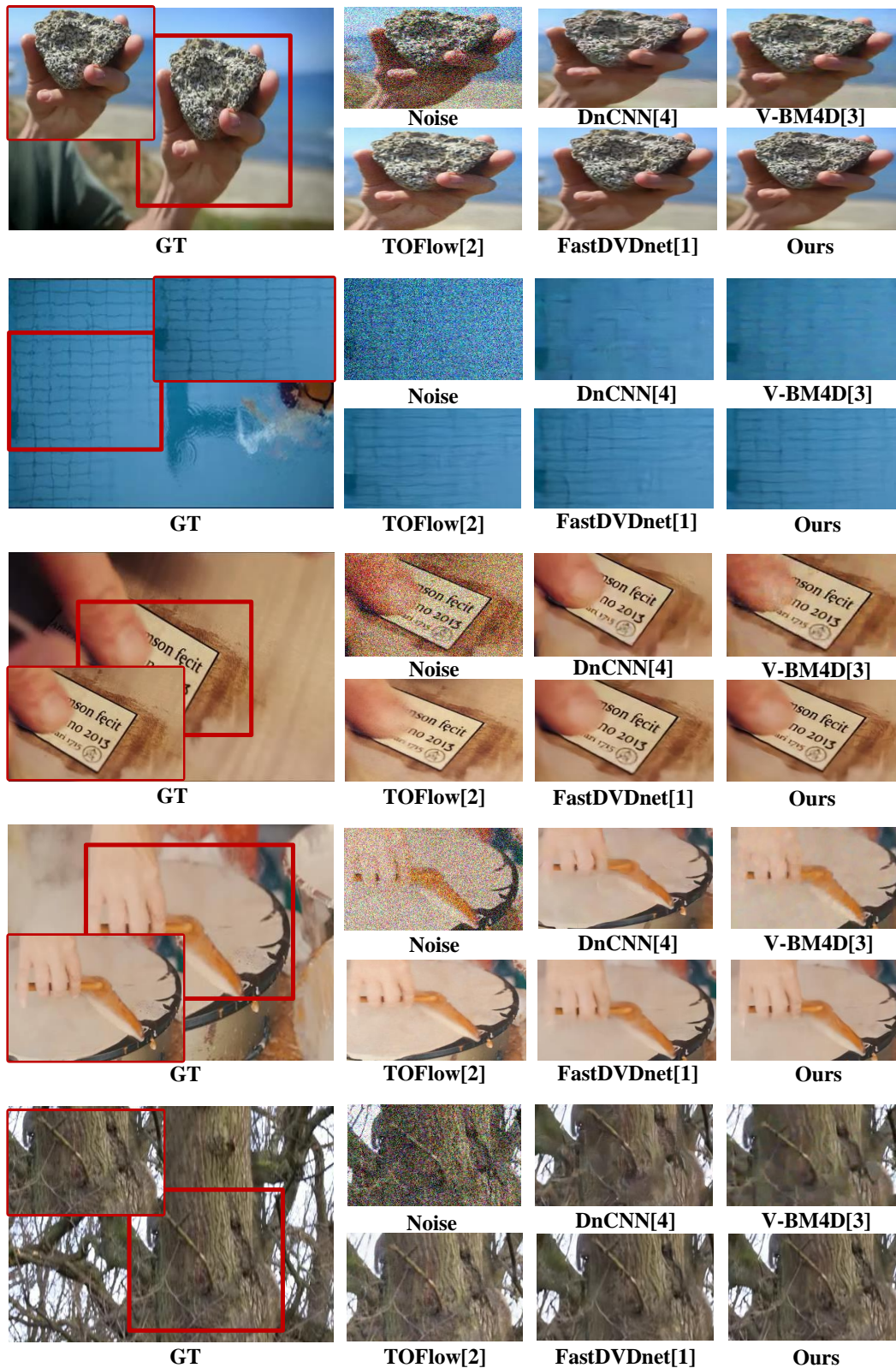


Figure 3: Denoising visualized results with Gaussian noise level $\sigma = 50$ on Vimeo90k dataset of the proposed DSCT and other state-of-the-art methods. From top to bottom shows different frames in a given video.

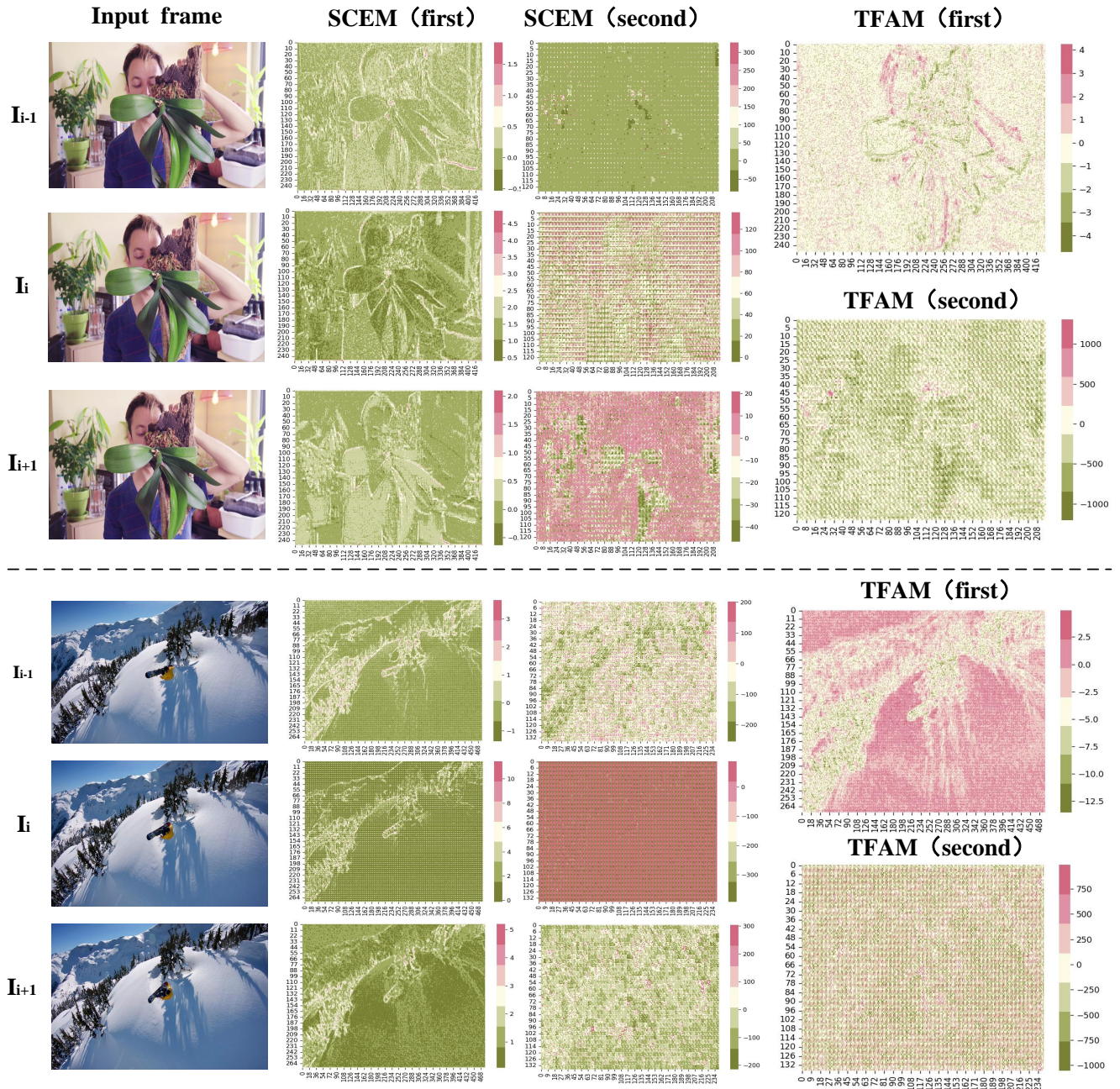


Figure 4: Visualization outputs of Spatial-Channel Encoding Module (SCEM) and Temporal Features Aggregation Module (TFAM). We show the features of the consecutive input frames after twice pass through SCEM and TFAM during the coarse-level stages. From top to bottom show video frames from Davis and Set8.

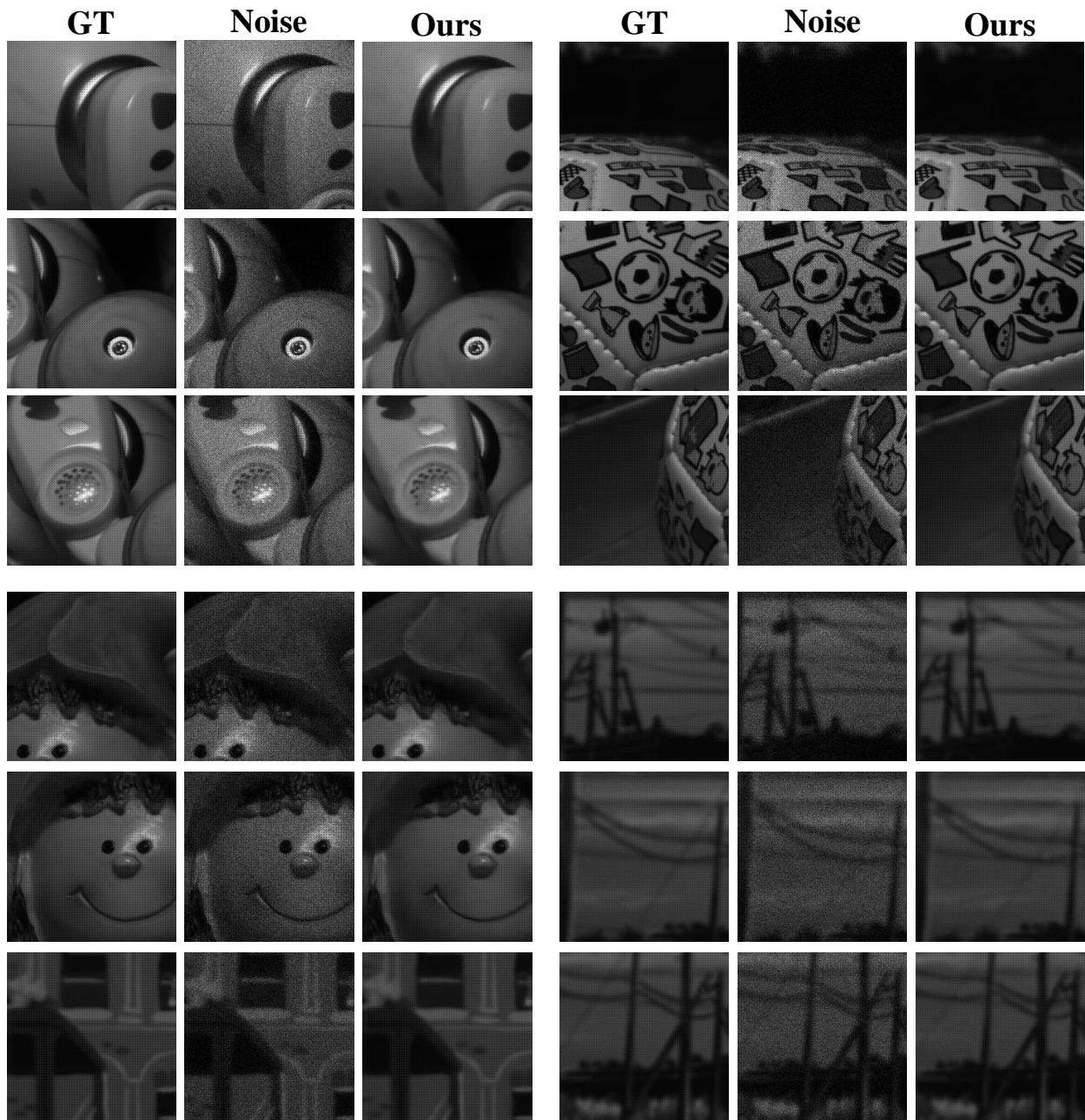


Figure 5: Denoising visualized results under ISO 25600 settings on the Raw videos dataset.